Journal of Surface Engineered Materials and Advanced Technology, **2013, 3, 18-26**
http://dx.doi.org/10.4236/jsemat.2013.33A004 Published Online September 2013 (http://www.scirp.org/journal/jsemat)

Surface Characterization of As-Spun and Supercontracted *Nephila clavipes* Dragline Silk

Benoit Faugas[1], Michael S. Ellison[1], Delphine Dean[2], Marian S. Kennedy[1]

[1]Department of Materials Science & Engineering, Clemson University, Clemson, USA; [2]Department of Bioengineering, Clemson University, Clemson, USA.
Email: mskenne@clemson.edu

Received June 20th, 2013; revised July 19th, 2013; accepted August 5th, 2013

ABSTRACT

Dragline spider silks have relatively high mass-based mechanical properties (tensile strength, elongation to break and rupture energy) and are environmentally responsive (supercontraction). In order to produce new synthetic fibers with these properties, many research groups have focused on identifying the chemical composition of these fibers and the structure of the fiber core. Since each fiber also has an outer skin, our study will provide a detailed understanding of the silk surface morphology, the response of the surface morphology to environmental conditions and processing variables, and also determine if the silk surface has a definitive patterning of charged amino acids. Specifically, by using force microscopy and functionalized nanoparticles, the present study examines 1) how the silk surface (topography, average roughness) is altered due to prior mechanical loading (viz. reeling speed), 2) alterations in morphology due to environmental conditions (supercontraction, storage time), and 3) the negatively and positively charged regions along with the surface using both force and nanoparticle mapping. Roughness data taken on dragline silk collected from *Nephila clavipes* spiders revealed that the surface comprised both smooth (5 nm RMS) and rough (65 nm RMS) regions. Supercontracted silk (from immersion in 0.01 M PBS during AFM testing) showed higher surface roughness values compared to spider silk tested in the air, indicating that the surface might be reorganized during supercontraction. No correlation was found between surface roughness and neither collection speed nor aging time for the as-spun or supercontracted fiber, demonstrating the surface stability of the dragline silk over time in terms of roughness. Both the force microscopy and the nanoparticle methods suggested that the density of negatively charged amino acids (glutamic acid, aspartic acid) was higher than that of the positively charged amino acids (lysine, asparagine, and histidine).

Keywords: Spider Dragline Silk; Surface Roughness; Supercontraction; Amino Acids; AFM; Force Microscopy; Nanoparticles

1. Introduction

Orb-weaver spiders, that is, spiders that produce spiral wheel-shaped prey-capture webs, are able to produce up to seven different types of silk. Each silk type has unique functions in the spider ecosphere including web structure, prey wrapping, or egg sack construction [1]. The most well studied silk type is dragline silk, due to its relatively high tensile strength (around 1.2 GPa) and large extensibility (around 18%), the combination of which results in a large work of rupture [2-9]. Interest in this silk is also due to its ability to respond to water. Unrestrained fibers have shown to shrink up to 60% in length relative to their as-spun state when either fully wetted [10,11] or subjected to a high relative humidity, *i.e*., above 70% - 75% [12-14]. This ability is termed supercontraction and is thought to be the result of breaking of the interchains hydrogen bonds in the amorphous regions of the fiber [12].

Dragline silk is produced in the spider's abdomen by the major ampullate gland. This silk is drawn through the spider's spinnerets and is a cylindrically shaped fiber with a diameter of three to five micrometers [9]. Researchers have shown that the fiber has three layers: a core, a skin and an outer layer. The outermost layer essentially comprises lipids and glycoproteins that fulfill an array of functions including protection against the environment, fortification again mico-organixms, carriers for pheromones in species recognition, water balance and lubricant [15,16]. The core includes many thread-like structures (fibrils), which are about 100 to 150 nm in size and are lined up along the fiber axis [16]. Inside these

fibrils, nanocrystallites are found attached together via a semi-amorphous domain [17].

Many studies have been performed to investigate chemical and structural composition of the entire fiber (core, skin and outer layer). The fiber contains two main proteins: the major ampullate spidroin 1 (MaSp1) and the major ampullate spidroin 2 (MaSp2). The primary structure of these proteins, *i.e.*, their amino acid sequence, has been identified: MaSp1 is made of a polyalanine block followed by a glycine-rich region made of GGA and GGX motifs (G = glycine, A = alanine, X = another amino acid) [18]; MaSp2 also has a polyalanine block but followed by GPGXX motifs (P = proline) [19]. These polyalanine blocks are organized in dense nanocrystallites and have an antiparallel β-sheet configuration [11, 20,21], whereas the semi-amorphous matrix has 31-helix type structures, α-helices and β-turns [21,22]. Currently, there are no published studies that focus on the structure of the skin.

This study will provide a detailed understanding of the silk surface morphology, *i.e.*, the shape and form of physical features on the surface and the response of the surface morphology in environmental conditions and processing variables, and will also determine if the silk surface has a definitive patterning of charged amino acids. Specifically, by using force microscopy and functionalized nanoparticles, the present study examines 1) how the silk surface (morphology, roughness) is altered due to prior mechanical loading (specifically the reeling speed), 2) alterations in morphology due to environmental conditions (supercontraction and storage time), and 3) the negatively and positively charged regions along the surface using both force mapping and SEM imaging of functionalized nanoparticles on the silk surface. It is more energetically stable to charge amino acids to be located on the surface of a protein rather than in the core, where the environment is neutral and hydrophobic [23].

2. Materials and Methods

2.1. Spider Dragline Silk Collection

Female *N. clavipes* spiders were collected near Charleston, South Carolina during the late summer months (July and August). These spiders were watered by misting their webs and fed with crickets each day. The dragline silk was artificially gathered on a metal spool with the use of a take-up reel [2] using the following steps. Each spider was sedated by cooling her in a refrigerator for one hour at approximately 4˚C. She was then rapidly transferred onto a foam block and attached with curved staples around her legs and body (**Figure 1**) [24]. The time to secure the spider was not enough to warm above 20˚C and it was assumed that temper during forced silking did not influence the dragline silk [25]. Once secured, the spider was put under the microscope and forceps were carefully brought inside the spinnerets. The silk was then pinched by the forceps and connected to the reel. Since spiders are thought normally to build their webs by producing silk at a rate between 10 - 20 mm/s [9,25], the collection speeds were selected around these values and will represent normal and abnormal production speeds. The dragline silk in this study was collected at rates representing normal collection speeds (14.0 mm/s), slower rates (0.7 and 2.2 mm/s) and faster rates (45.7 and 65.1 mm/s). The silk was collected between six months and seven years before testing and was then stored inside a dark cabinet at room temperature and humidity. By characterizing a range of speeds and aging times, this work will allow researchers to compare between published results that do not identify or contain varied reeling conditions and/or silk storage time.

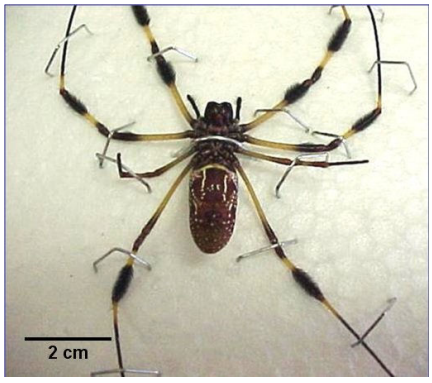

Figure 1. ***N. clavipes*** **spider restrained onto a Styrofoam block for silk collection.**

2.2. Surface Morphology Characterization of Spider Dragline Silk

To characterize both the surface morphology and roughness of the collected silk, an atomic force microscope (Veeco Dimension 3100, Digital Instruments) was used. Scans were completed both in air and aqueous fluid to compare the silk surface morphology in the as-spun and supercontracted states respectively. Contact mode scans were run using silicon nitride cantilevers (spring constant—0.12 N/m, resonant frequency between 14 kHz and 26 kHz) in both air and fluid (0.01 M of Phosphate Buffer Saline). To increase the rigidity of the silk fibers during scanning, fibers were straightened and adhered to the slide by placing Loctite® glue beads onto the fiber at 5 mm intervals. The average strain of these fibers was 8.7%. Fibers tested in the PBS solution were in the supercontracted state. In our case of restrained fibers, supercontraction still occurred and internal forces were induced [12-14]. All roughness measurements were made using either 1 μm or 2 μm scan boxes. Previous work has

shown that the scan size influences the reported AFM roughness value [26]; therefore values were only compared between identical scan sizes. To compare roughness without the influence of individual fiber diameters, a 2nd order fit was applied to every scan in order to remove the curvature and then average roughness (R_a) values were calculated using the instrument software (NanoScope v613r1). Before characterizing the surface morphology and surface roughness, initial tests were completed to determine the sampling influence and possible wear. These tests were run using a supercontracted fiber. Five scans over a 1 μm × 1 μm area were run and then the scan size area was enlarged to 2 μm × 2 μm.

2.3. Determination of Surface Charge Density Spacial Distribution and Labeling of Charged Amino Acids with Gold Nanoparticles

Both force mapping and nanoparticle labeling methods were used to identify the arrangement of positively and negatively charged amino acids. For charge density mapping, a cantilever tip was functionalized with carboxyl or amine groups. An array of force-distance curves was taken and then was analyzed to generate a force map using the linear Poisson-Boltzmann model equation:

$$F = 4\pi R_{\text{tip}} \frac{\sigma_{\text{tip}}\sigma_{\text{fiber}}}{\varepsilon_w \kappa} e^{-(\kappa D)} \quad (1)$$

where R_{tip} (25 nm) is the radius of the tip, σ_{tip} is the charge density on the tip, σ_{fiber} is the charge density on the fiber, ε_w is the permittivity of the fluid ($6.923 * 10^{-10}$ C^2/Nm^2), κ^{-1} is the Debye length and D is the tip-sample separation distance. The surface charge density of the carboxyl-terminated tips has been previously measured and was found to be −0.01 C/m^2 [27] and the Debye length in 0.01 M PBS is approximately 3 nm [28]. For this study, 500 nm × 500 nm square arrays with 20 force-distances curves were taken on each of the 20 rows. This resulted in a force-distance curve being taken each 25.6 nm. This method was outlined in detail within previous publications [28,29].

To corroborate the data from force mapping method, a second technique using nanoparticle markers was used. Gold nanoparticles (Cytodiagnostics, 20 nm diameter) were functionalized with carboxyl groups (respectively amine groups) using 11-mercaptoundecanoic acid (respectively using 11-Amino-1-undecanethiol) to allow the identification of positively (respectively negative) charged amino acids. The solution was poured on the unstretched restrained fiber. EDC and Sulfo-NHS were added and allowed to react for 2 h at 37˚C, hereby attaching the functionalized gold nanoparticles to the targeted amino acids via a stable peptide bond [30]. The fibers samples were then washed several times in 0.1 M PBS using sonication for 10 min at 50/60 Hz. To image the arrangement of the nanoparticles, the Hitachi SU6600 scanning electron microscope in the Clemson University Electron Microscope Facility in the Advanced Materials Research Laboratory was used in backscatter mode, utilizing the variable pressure environment capabilities of the SU660 to reduce charging effects.

3. Results and Discussion

3.1. Reproducibility of Measurements

The reproducibility of measurements and measurement artifacts were considered carefully. To calculate the surface roughness for both the as-spun and supercontracted states, contact AFM was utilized. Potential errors from this method could have included plowing (scraping) of the tip during scanning, scanning drift and/or sampling errors. Plowing could be produced when scanning a soft sample during contact mode. Dragline silk samples tested in both air and PBS did not show wear boxes (**Figure 2**), which would have resulted if plowing had occurred. The silk used in these experiments was foced at a speed of 45.7 mm/s and were preformed in PBS (supercontracted state). **Figure 2** showed a fiber scanned initially with a 1 μm scanning box and subsequently using a 2 μm box centered over the original 1 μm scanning box. In the 2 μm scan, there was no evidence of the prior 1 μm scan and the morphology did not change (the higher features were identical between scans). However, scanning the same area sequentially was affected by drift illustrated with a shift of the features towards the upper left as seen in **Figure 3**. **Figure 4** showed the average R_a roughness as a function of the sequential scan number (both 1 μm and 2 μm scan boxes). This plot showed that the roughness value changes with each scan number. Since no wear was present (demonstrated in **Figure 2**), this change was attributed to the drift (demonstrated in **Figure 3**).

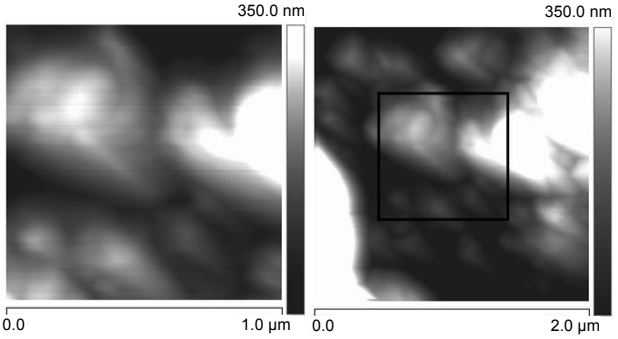

Figure 2. A square of 1 μm area (left) was scanned with a high set point and then reimaged at 2 μm (right). The black box in the right height image matches the area of the left height image. Comparison of these AFM scans shows no evidence of surface wear on the supercontacted spider dragline silk resulting from the AFM tip.

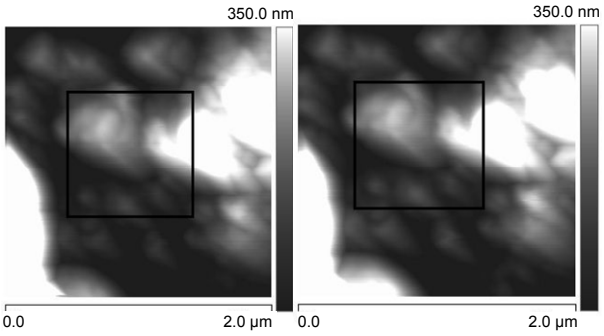

Figure 3. The surface of the spider silk (collected at a rate of 45.7 mm/s) was scanned repetitively using the AFM. Comparing the right and left height images show some drift with the features being shifted to the upper left.

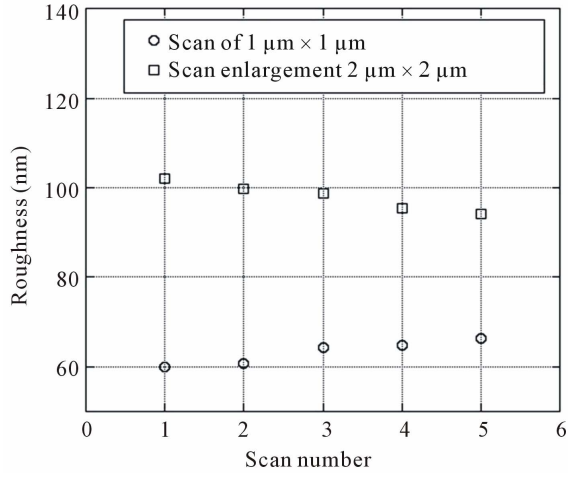

Figure 4. Sequential scans (five) taken of the same area at two different scan sizes (1 µm × 1 µm and 2 µm × 2 µm). The drift indicated in Figure 3 results in small changes to the surface roughness values. This silk had a reeling speed of 45.7 mm/s and was in the supercontracted state.

3.2. Surface Morphology of As-Spun and Supercontracted Spider Dragline Silk

The fiber surface scans provided a better understanding of the dragline fiber morphology in both the as-spun and supercontracted fibers. There were two distinct surface morphologies present along both the as-spun (**Figure 5**) and supercontracted fibers (**Figure 6**). These comparesons were made using dragline fiber reeled at 65.1 mm/s and collected six years before testing. One surface type had large (400 nm diameter) globules present (**Figure 6**) and the second had small spherical features of 40 nm diameter (**Figure 5**). The large globules having extended heights on the surface were randomly spread, thus they can be attributed to lipids and/or glycoproteins attached to the skin below, in accordance with the vision of surface layers reported by Sponner's *et al.* [13]. The small spherical features were lined up along the longitudinal fiber axis, which was similar to the findings of Du on *N. pilipes* spiders [31]. Furthermore, it has been noticed on several of our AFM images taken in aqueous fluid that there were some cracks on the surface, generally oriented along the fiber axis (like the black "worm" lines on **Figure 6**). Since spider silk was known to have a skin-core structure with fibrils inside the core, this crack could have been in fact a fibril. However, if we were able to see the fibrils, we would have seen more than one fibril that composed the core, so this was not a likely explana-

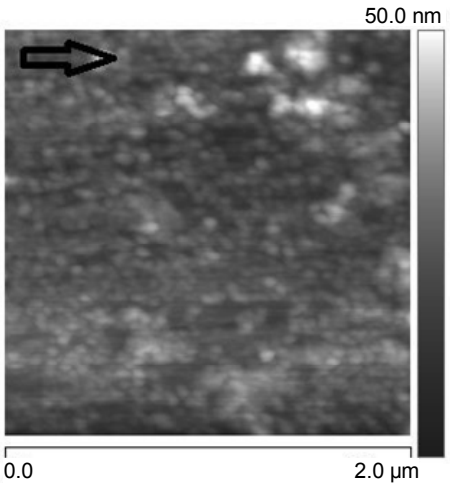

Figure 5. Representative AFM scan (height) of the surface of as-spun (non-supercontracted) *N. clavipes* dragline silk. The surface appears to have small beads that line up along the fiber (the arrow indicates the longitudinal fiber axis) and the surface roughness (R_a) is 4.4 nm. This silk was extracted at a reel rate of 65.1 mm/s.

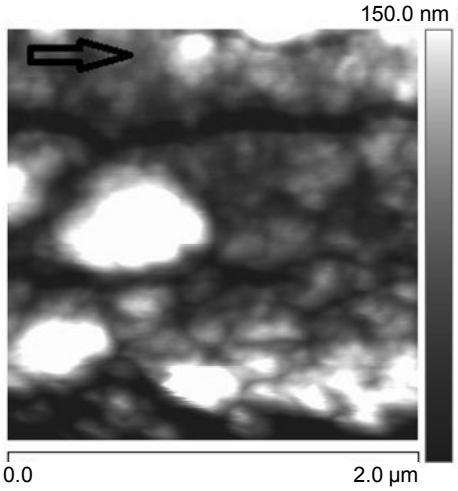

Figure 6. Representative AFM scan images (height) taken along the surface of supercontracted *N. clavipes* dragline silk. Distinct globular shapes are evident, which likely localized glycoproteins and/or lipids. Deep ridges are also shown to run parallel to the longitudinal fiber axis (indicated with arrow). This silk was collected at a reeling rate of 65.1 mm/s and the resulting surface roughness (R_a) is 63.5 nm.

tion. Moreover, a skin cladding surrounded the core and this would have prevented the AFM from seeing the core. Thus, a possible explanation was that this outer skin may have been releasing some stress by forming these cracks. Since the fiber was stretched, both during the silking operation and the sample preparation (and by the supercontraction phenomenon to a lesser extent), this cracking may have been a result of stretching the fiber above its surface yield elongation point during the sample preparation. This could correlate with the results of Zax *et al.* [7] who found that a splitting was occurring along and across the fiber axis after tensile testing.

The response of the surface roughness to the environment was detected by measuring the silk in air and aqueous fluid. Both as-spun and supercontracted fibers showed smooth and rough regions. However, the smooth regions (R_a ranging between 0 and 20 nm) were more prevalent in the as-spun samples (31% as shown in **Figure 7**) than in the supercontracted samples (7% as shown in **Figure 8**). Supercontraction is known to make spider silks shrink; thus, we may have expected to see an increase in surface roughness when the pre-stressed proteins contract by making the lengthened chains go higher in height (relative to the surface) in response to their reduction in length. A t-test performed for the roughness values between the as-spun and the supercontracted state lead to [$P(T \leq t)$ two-tail] = 2.06×10^{-7}, which was less than 0.05. Thus, supercontraction significantly increased surface roughness. Even though proteins may have been different on the surface, they still were affected by supercontraction and went through conformational changes.

In addition to the influence of moisture in the silk environment, the collection speed effect on surface roughness was determined. Measurements taken along as-spun dragline silk obtained at reeling speeds of 0.7, 2.2, 14.0, 45.7 and 65.1 mm/s (**Figure 9**) showed that the average roughness did not change within this range of collection speed. The same result was obtained for supercontracted silk (**Figure 10**). It is important to note that the roughness values reported in our study may not have been the "exact" values because of the scan size area used and also because of the Planefit process used to remove the arch shaped bow on the images. However, since every image was taken with the same scan size of 2 μm × 2 μm and was treated with a 2nd order Planefitting, the trend reported was valid.

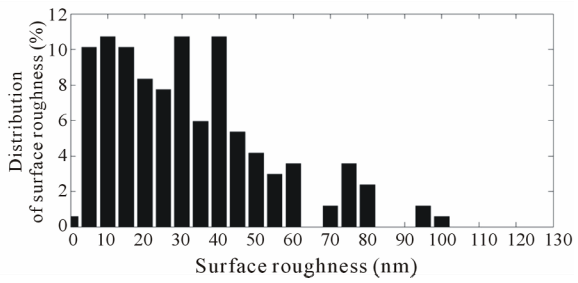

Figure 7. Distribution of surface roughness values for *N. clavipes* silk tested in air. The width of each bar is 5 nm.

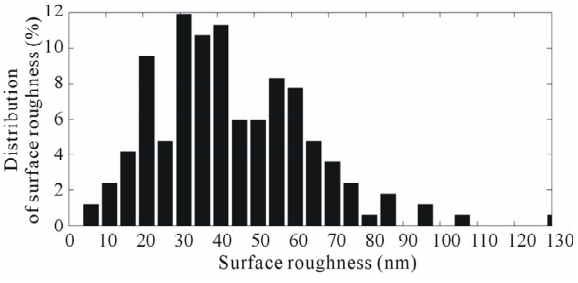

Figure 8. Distribution of surface roughness values for *N. clavipes* silk tested in 0.01 M PBS (supercontracted state). Comparison with Figure 7 shows that the distribution changes as fibers transition from the as-spun to supercontracted states. The width of each bar is 5 nm.

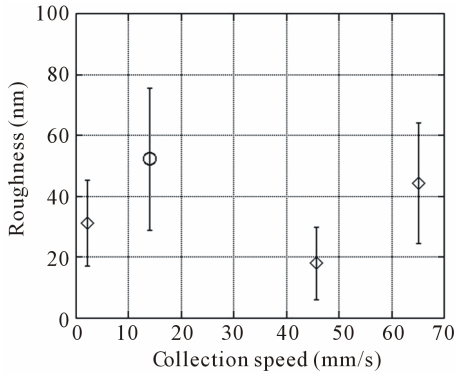

Figure 9. Average roughness values obtained using 42 individual AFM scans at each collection speed showed that the surface roughness of the as-spun silk (non-supercontracted) was independent of collection speed. The diamonds represent a five-year-old spider silk whereas circle represents fresh spider silk.

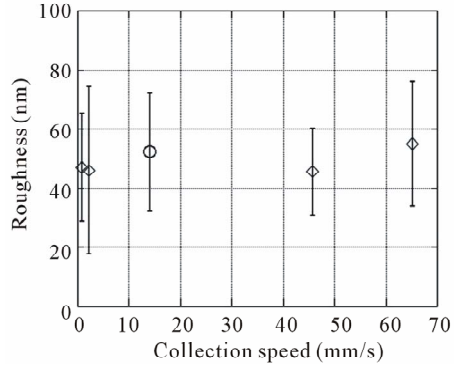

Figure 10. Surface roughness of supercontracted silk (averaged from 42 individual scans at each collection speed) is independent of collection speed. Roughness values were obtained using AFM scans. The diamonds represent a five year-old spider silk whereas circle represents fresh spider silk.

Along with collection speed consequences on surface roughness, the aging time effect (*i.e.*, time since silk collection) was investigated. The silk reeled at 14 mm/s was collected six months to one year before testing compared to the other silks that were collected at least five years before testing. Data showed (**Figures 9** and **10**) that the the surface roughness values of this "fresh" silk did not differ from the "old" silk. This implied that this fiber aging did not affect spider silk surface roughness, and demonstrated the surface stability of the dragline silk over time in terms of roughness. Thus, surface roughness did not change when increasing collection speed nor when aging, whether the silk was in the supercontracted state or not.

3.3. Surface Identification of Charged Amino Acids and Spatial Distribution of Surface Charge Density

Sponner *et al.* [13] suggested within dragline silk fibers the layer just below the lipid and glycoprotein coat comprised proteins having a sequence that was similar to that of the minor ampullate silk used by spiders for web reinforcement. Since the primary structure of the dragline silk consists of regular alanine and glycine repeat units in the core, we tried to determine if a pattern for the electrically charged amino acids may be seen on the surface in terms of spatial frequency. In order to look at the charged amino acids and their spatial distribution, a map of surface charge densities was obtained through the use of AFM force-distance curves taken in a 500 nm box. The revealed representative map of surface charge densities in **Figure 11(a)**, showed darker squares as negative surface charge densities and white squares as positive (or neutral) surface charge densities. It is crucial to note that when performing force-distance curves the size of the AFM tip implied that it interacted with more than one amino acid on the surface, and thus the surface charge density values unveiled an average of all the interactions between the tip and the surrounding amino acids. Therefore, darker squares represented regions having interactions with more negatively charged amino acids than positively charged amino acids. Plus, force-distance curves were taken 25.6 nm apart and the radius of the tip was 50 nm; thus measurements taken next to each other partially probed several amino acids. Moreover, the tip-surface interaction occurred at one point in space (1D) but the surface charge density value obtained was extended to a square (2D) in order to get a visual map. The map given in **Figure 11(a)** did not show a regular pattern in the spatial distribution of surface charge densities. Then charged amino acids may be seen as randomly spread on the sub-micron scale. However, a much smaller tip would be required to probe them individually on the nanoscale. Furthermore, we did not report any correlation between the surface charge densities shown in the map and special features on the associated AFM height image (see **Figure 11(b)**). Though, it is important to note that a drift has been identified when scanning the silk surface; thus, the force map might have been taken with a small shift relative to the AFM image and change our vision of a possible match between surface charge densities and features.

The quantitative distribution of surface charge density values given in **Figure 12** revealed a slight predominance of negative surface charge densities around −0.2 C/m^2. Values around −0.3 C/m^2 corresponded to values close to the control, where AFM force-distance curves were taken on a silicon wafer coated with gold and functionalized with carboxyl groups; thus force-distance curves leading to surface charge densities values around −0.2 C/m² probe more than one negatively charged

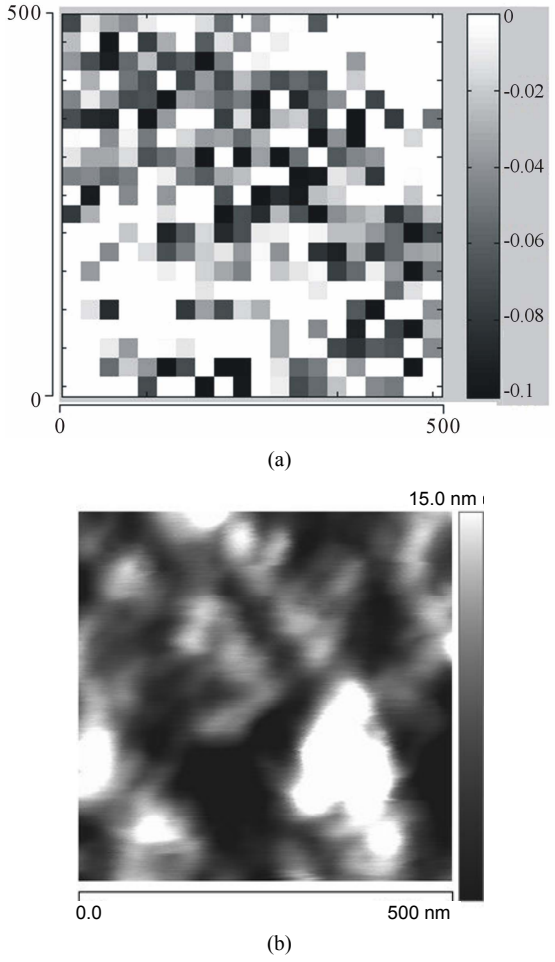

Figure 11. (a) This representative image is a surface charge density map of supercontracted spider silk. The negative surface charge density areas (darker squares) are more prevalent than are the positive ones (white squares). The scale bar is in C/m^2, and positive values (in white) are omitted from the scale bar for visual clarity; x and y axes are in nm. (b) The associated AFM height image.

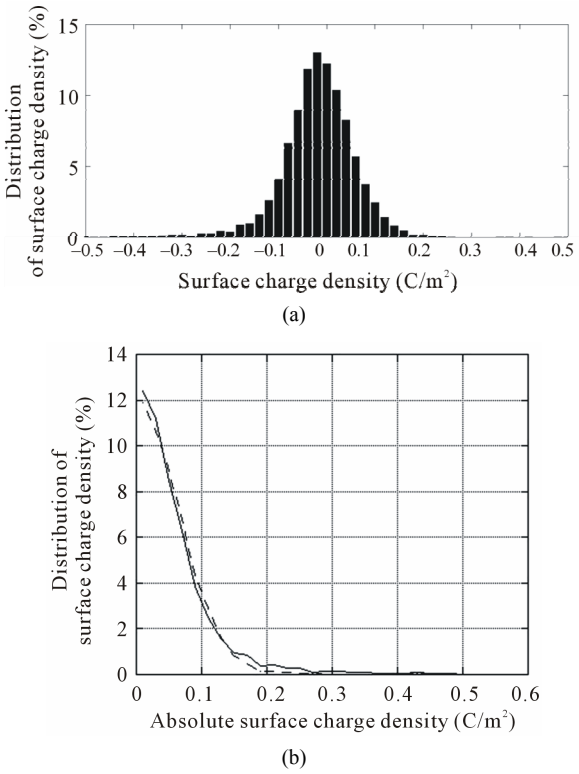

Figure 12. (a) Distribution of surface charge density values for *N. clavipes* silk tested in 0.01 M PBS (supercontracted state). This silk was collected at a rate of 14 mm/s. The width of each bar is 0.02 C/m^2. 13% of all the surface charge density values (maximum peak) are comprised between −0.02 C/m^2 and 0 C/m^2. (b) Comparative distribution of positive (dotted line) and negative (continuous line) surface charge densities taken from the data in (a) as a function of absolute charge density.

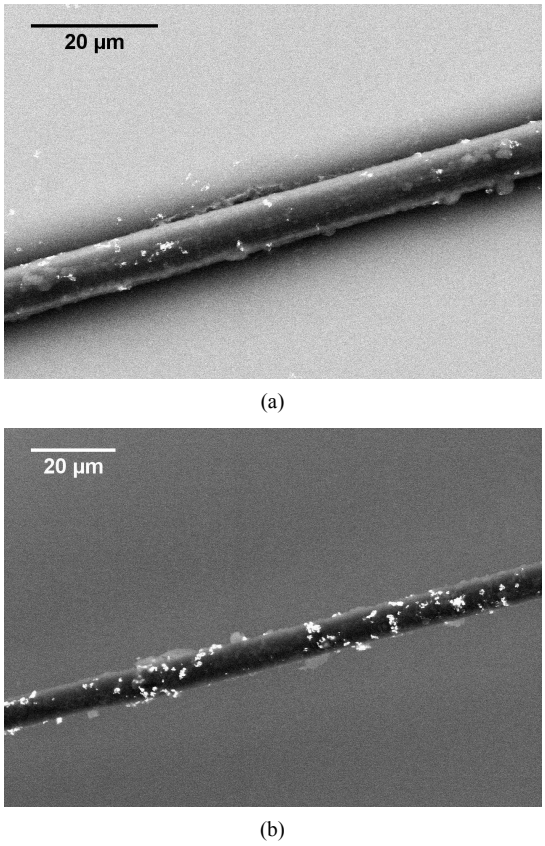

Figure 13. (a) SEM images of silk fibers exposed to solutions of PBS and surface modified gold nanoparticles. (a) This representative image of fibers with negatively charged nanoparticles indicate that the positively charged amino acids are randomly spread along the fiber surface. (b) This image shows that the negatively charged amino acids (marked with the positively charged nanoparticles) are more densely packed. The silk used in these tests was collected at 0.7 mm/s and was collected six years before testing.

amino acid, and this also meant that they can be spread a few nanometers apart. Hence, there were more negatively charged amino acids found on the surface compared to positively charged amino acids.

In order to check the previous findings obtained with force mapping, scanning electron microscopy images of single spider dragline silk (supercontracted) coated with gold nanoparticles functionalized with COOH and NH_2 were taken (**Figure 13**). In **Figure 13(a)**, the image displayed a fiber treated with COOH functionalized gold nanoparticles that attached specifically to the positively charged amino acids lysine, arginine and histidine. In **Figure 13(b)**, the image depicted a fiber treated with NH_2 functionalized gold nanoparticles that attached specifically to the negatively charged amino acids glutamic acid and aspartic acid. These SEM images for amino acid surface characterization revealed a higher amount of negatively charged amino acids spread over the surface (**Figure 13(b)**) compared to positively charged amino acids (**Figure 13(a)**), confirming the findings with force mapping. This result also correlates with the findings from bulk amino acid analysis that showed that negatively charged amino acids were found in a higher amount than the positively charged amino acids [2,20,32]. A possible pattern can be seen on the image of **Figure 13(b)** that located the negatively charged amino acids. It was seen that gold nanoparticles were arranged as if forming a helix around the fiber. Other images coming from this same fiber also showed this type of arrangement at different locations, but in another report, the fiber analyzed did not show this pattern at all [23]. Images that located positively charged amino acids did not demonstrate any pattern, and these amino acids were spread randomly on the surface. It could be seen that there were some gold nanoparticles trapped between the fiber and the microscope slide. These gold nanoparticles might not have been attached to the targeted amino acids since they might have been only gold nanoparticles that could have not been removed by washing. It is also important to notice that we only saw about half of the fiber because the

other half was "stuck" to the microscope slide. Hence, we did not have access to information regarding the fiber structure between the fiber and microscope slide, and it is clear that we were missing the targeted amino acids. Furthermore, it is interesting to consider that in our experiments fibers were subjected to supercontraction before the attachment of gold nanoparticles. Indeed, restrained fibers were in contact with the aqueous gold nanoparticles solution before the peptide bond reaction could occur. This means that protein chains on the surface were allowed to reorient and change conformation due to supercontraction, as suggested by our roughness experiments. Thus, the side-chains of charged amino acids may have been available on the surface (or unavailable if they turned inside) for gold nanoparticles to attach. Hence, SEM images may have not shown all the charged amino acids present on the surface. It is also worth noting that some clusters of gold nanoparticles can be identified on the dragline silk surface. It is unlikely that the entire surface covered by the cluster contain the type of amino acids we were looking at, meaning that we would have had a polypeptide chain with a long sequence of glutamic/aspartic acid. However, these clusters were micrometers wide and hid a certain amount of these amino acids since negatively charged amino acids can be found few nanometers apart, as demonstrated by the force microscopy experiments. Thus, these clusters affected the vision we had of their distribution.

4. Conclusion

This study determined the surface morphology of artificially forced *N. clavipes* spider dragline silk through the use of atomic force microscopy. The silk surface, in both the as-spun and supercontracted states, showed large and small globule surface features and exhibited different level of roughness ranging from 5 nm to 65 nm. A relatively large surface roughness was measured when the spider silk was tested in a water-based environment, indicating that proteins on the surface were affected by the supercontraction process. Although changes in environment resulted in roughness alteration, there was no correlation between the collection speed and or the collection time with the roughness for in either the as-spun or supercontracted states. Characterization of the chemical composition of the *N. clavipes* dragline silk surface showed that both positively and negatively charged amino acids are present on the surface. The areal density of negatively charged amino acids (glutamic acid and aspartic acid) was higher than the positively charged ones (lysine, asparagine, and histidine). Initial results indicate that the negatively charged amino acids were spaced regularly at some locations along the fiber, while the positively charged amino acids did not show a patterned arrangement appearing randomly arranged on the surface.

5. Acknowledgements

The authors would like to thank Mr. Donald Mulwee of the Clemson University Electron Microscopy facility for discussions on sample preparation and imaging conditions. In addition, they would like to acknowledge Mr. Matthew Marchewka and Mr. Joseph Durst for helpful discussions as well as Mr. Godfrey Kimball for useful editorial comments on this manuscript. This project was partially funded by the Atlantis MILMI program, which supports the cooperation between EU and US higher education institutions. Funding support was also provided by the US Department of Education under contract #P116J080033 (University of Central Florida) and the European Commission under contract #2008-1750/001-001 CPT-USTRAN (Université Bordeaux 1) and by the Clemson University Department of Materials Science and Engineering.

REFERENCES

[1] F. Vollrath, "Strength and Structure of Spiders' Silks," *Reviews in Molecular Biotechnology*, Vol. 74, No. 2, 2000, pp. 67-83. doi:10.1016/S1389-0352(00)00006-4

[2] J. C. Zemlin, "A Study of the Mechanical Behavior of Spider's Silks," Technical Report 69-29-CM, AD 684333, US Army Natick Laboratories, Natick, 1968.

[3] R. W. Work, "The Force-Elongation Behavior of Web Fibers and Silks Forcibly Obtained from Orb-Web-Spinning Spider," *Textile Research Journal*, Vol. 46, 1976, pp. 485-492.

[4] J. M. Gosline, P. A. Guerette, C. S. Ortlepp and K. N. Savage, "The Mechanical Design of Spider Silks: From Fibroin Sequence to Mechanical Function," *The Journal of Experimental Biology*, Vol. 202, 1999, pp. 3295-3303.

[5] S. L. Stauffer, S. L. Coguill and R. V. Lewis, "Comparison of Physical Properties of three Silks from *Nephila clavipes* and *Araneus Gemmoides*," *The Journal of Arachnology*, Vol. 22, No. 1, 1994, pp. 5-11.

[6] M. Hudspeth, X. Nie, W. N. Chen and R. V. Lewis, "Effect of Loading Rate on Mechanical Properties and Fracture Morphology of Spider Silk," *Biomacromolecules*, Vol. 13, No. 8, 2012, pp. 2240-2246. doi:10.1021/bm3003732

[7] D. B. Zax, D. Armanios, S. Horak, C. Malowniak and Z. Yang, "Variation of Mechanical Properties with Amino Acid Content in the Silk of *Nephila clavipes*," *Biomacromolecules*, Vol. 5, No. 3, 2004, pp. 732-738. doi:10.1021/bm034309x

[8] B. O. Swanson, T. A. Blackledge, J. Beltran and C. Y. Hayashi, "Variation in the Material Properties of Spider Dragline Silk Across Species," *Applied Physics A*: *Materials Science & Processing*, Vol. 82, No. 2, 2006, pp. 213-218. doi:10.1007/s00339-005-3427-6

[9] P. M. Cunniff, S. A. Fossey, M. A. Auerbach, J. W. Song,

D. Kaplan, W. W. Adams, R. K. Eby, D. Mahoney and D. L. Vezie, "Mechanical and Thermal Properties of Dragline Silk from the Spider *Nephila clavipes*," *Polymers for Advanced Technologies*, Vol. 5, No. 8, 1994, pp. 401-410. doi:10.1002/pat.1994.220050801

[10] R. W. Work, "A Comparative Study of the Supercontraction of Major Ampullate Silk Fibers of Orb-Web-Building Spiders (Araneae)," *Journal of Arachnology*, Vol. 9, No. 3, 1981, pp. 299-308.

[11] L. W. Jelinski, A. Blye, O. Liivak, C. Michal, G. LaVerde, A. Seidel, N. Shah and Z. Yang, "Orientation, Structure, Wet-Spinning, and Molecular Basis for Supercontraction of Spider Dragline Silk," *International Journal of Biological Macromolecules*, Vol. 24, No. 2-3, 1999, pp. 197-201. doi:10.1016/S0141-8130(98)00085-3

[12] T. A. Blackledge, C. Boutry, S. C. Wong, A. Baji, A. Dhinojwala, V. Sahni and I. Agnarsson, "How Super Is Supercontraction? Persistent versus Cyclic Responses to Humidity in Spider Dragline Silk," *Journal of Experimental Biology*, Vol. 212, No. 13, 2009, pp. 1980-1988. doi:10.1242/jeb.028944

[13] K. N. Savage, P. A. Guerette and J. M. Gosline, "Supercontraction Stress in Spider Webs," *Biomacromolecules*, Vol. 5, 2004, pp. 675-679. doi:10.1021/bm034270w

[14] I. Agnarsson, P. A. Guerette and J. M. Gosline, "Supercontraction Forces in Spider Dragline Silk Depend on Hydration Rate," *Zoology*, Vol. 112, No. 5, 2009, pp. 325-331. doi:10.1016/j.zool.2008.11.003

[15] A. Sponner, W. Vater, S. Monajembashi, E. Unger, F. Grosse and K. Weisshart, "Composition and Hierarchical Organization of a Spider Silk," *PloS One*, Vol. 2, No. 10, 2007, pp. 1-8. doi:10.1371/journal.pone.0000998

[16] K. Augsten, P. Mühlig and C. Herrmann, "Glycoproteins and Skin-Core Structure in *Nephila clavipes* Spider Silk Observed by Light and Electron Microscopy," *Scanning*, Vol. 22, 2000, pp. 12-15. doi:10.1002/sca.4950220103

[17] L. Eisoldt, A. Smith and T. Schiebel, "Decoding the Secrets of Spider Silk," *Materials Today* (*Kidlington*, *England*), Vol. 14, No. 3, 2011, pp. 80-86.

[18] M. Xu and R. V. Lewis, "Structure of a Protein Superfiber: Spider Dragline Silk," *Proceedings of the National Academy of Sciences*, Vol. 87, No. 18, 1990, pp. 7120-7124. doi:10.1073/pnas.87.18.7120

[19] M. Hinman, J. Jones and R. V. Lewis, "Synthetic Spider Silk: A Modular Fiber," *Trends in Biotechnology*, Vol. 18, No. 9, 2000, pp. 374-379. doi:10.1016/S0167-7799(00)01481-5

[20] J. O. Warwicker, "Comparative Studies of Fibroins: II. The Crystal Structures of Various Fibroins," *Journal of Molecular Biology*, Vol. 2, 1960, pp. 350-362. doi:10.1016/S0022-2836(60)80046-0

[21] M. Creager, J. E. Jenkins, L. A. Thagard-Yeaman, A. E. Brooks, J. A. Jones, R. V. Lewis, G. P. Holland and J. L. Yarger, "Solid-State NMR Comparison of Various Spiders' Dragline Silk Fiber," *Biomacromolecules*, Vol. 11, No. 8, 2010, pp. 2039-2043. doi:10.1021/bm100399x

[22] J. D. Van Beek, S. Hess, F. Vollrath and B. H. Meier, "The Molecular Structure of Spider Dragline Silk: Folding and Orientation of the Protein Backbone," *PNAS*: *Proceedings of the National Academy of Sciences*, Vol. 99, No. 16, 2002, pp. 10266-10271.

[23] R. H. Garrett and C. M. Grishman, "Biochemistry," Brooks/Cole, 1999.

[24] B. Faugas, "Surface Characterization of *Nephila clavipes* Dragline Silk," Master's Thesis, Clemson University, Clemson, 2012.

[25] F. Vollrath, B. Madsen and Z. Shao, "The Effect of Spinning Conditions on the Mechanics of a Spider's Dragline Silk," *Proceedings of the Royal Society B*: *Biological Sciences*, Vol. 268, No. 1483, 2001, pp. 2339-2346. doi:10.1098/rspb.2001.1590

[26] P. J. Ramón-Torregrosa, M. A. Rodríguez-Valverdea, A. Amirfazlia and M. A. Cabrerizo-Vílcheza, "Factors Affecting the Measurement of Roughness Factor of Surfaces and its Implications for Wetting Studies," *Colloids and Surfaces A*: *Physicochemical and Engineering Aspects*, Vol. 323, No. 1-3, 2008, pp. 83-93. doi:10.1016/j.colsurfa.2007.10.032

[27] J. Vandiver, D. Dean, N. Patel, W. Bonfield and C. Ortiz, "Nanoscale Variation in Surface Charge by Synthetic Hydroxyapatite Detected by Chemically and Spatially Specific High Resolution Force Spectroscopy," *Biomaterials*, Vol. 25, No. 3, 2005, pp. 271-83. doi:10.1016/j.biomaterials.2004.02.053

[28] B. Zimmerman, J. Chow, A. G. Abbott, M. S. Ellison, M. S. Kennedy and D. Dean, "Variation of Surface Charge Along the Surface of Wool Fibers Assessed by High-Resolution Force Spectroscopy," *Journal of Engineered Fibers and Fabrics*, Vol. 6, No. 2, 2011, pp. 61-66.

[29] B. Zimmerman, "Mechanical and Chemical Characterization of Biological Composite Structures," Master's Thesis, Clemson University, Clemson, 2009.

[30] G. T. Hermanson, "Bioconjugate Techniques," Academic Press, Boston, 2008.

[31] N. Du, Z. Yang, X. Y. Liu, Y. Li and H. Y. Xu "Structural Origin of the Strain-Hardening of Spider Silk," *Advanced Functional Materials*, Vol. 21, No. 4, 2011, pp. 772-778. doi:10.1002/adfm.201001397

[32] S. Lombardi and D. Kaplan, "The Amino Acid Composition of Major Ampullate Gland Silk (Dragline) of *Nephila clavipes* (Araneae, Tetragnathidae)," *Journal of Arachnology*, Vol. 18, No. 3, 1990, pp. 297-306.

